Coffee Waste-Derived Hierarchical Porous Carbon as a Highly Active and Durable Electrocatalyst for Electrochemical Energy Applications

Dong Young Chung,[†,‡,§] Yoon Jun Son,[†,‡,§] Ji Mun Yoo,[†,‡,§] Jin Soo Kang,[†,‡] Chi-Yeong Ahn,[†,‡] Subin Park,[†,‡] and Yung-Eun Sung*[†,‡]

[†]Center for Nanoparticle Research, Institute for Basic Science (IBS), Seoul 08826, Republic of Korea
[‡]School of Chemical and Biological Engineering, Seoul National University (SNU), Seoul 08826, Republic of Korea

Supporting Information

ABSTRACT: Nitrogen-doped porous carbon materials have been highlighted as promising alternatives to high-cost platinum in various electrochemical energy applications. However, protocols to generate effective pore structure are still challenging, which hampers mass production and utilization of carbon materials. Here, we suggest a facile and effective method for hierarchical porous carbon by a single-step carbonization of coffee waste (CW) with $ZnCl_2$. The CW, which is one of the most earth-abundant organic waste, can be successfully converted to nitrogen-doped porous carbon. It shows outstanding oxygen reduction activity and durability comparable to the state-of-the-art platinum, and the half-wave potential is also comparable to the best metal-free electrocatalysts in alkaline media. Finally, we apply it to counter electrode of dye-sensitized solar cell, whose photovoltaic efficiency surpasses the one made with conventional platinum electrode. We demonstrate the feasibility of our strategies for highly efficient, cheap, and environment-friendly electrocatalyst to replace platinum in various electrochemical energy applications.

KEYWORDS: nitrogen-doped carbon, coffee waste, hierarchical porous structure, oxygen reduction reaction, dye-sensitized solar cell

1. INTRODUCTION

Development of renewable energy sources has recently been regarded as an important issue because of limited fossil fuel reserves and severe environmental aggravation. Among various candidates, electrochemical-based energy conversion and storage devices are promising solutions to the recent energy and environmental crises. In many electrochemical energy fields, such as fuel cells and dye-sensitized solar cells (DSSCs), platinum (Pt) has been widely used as an efficient electrocatalyst for oxygen reduction reaction (ORR)[1,2] and triiodide reduction reaction (IRR).[3] However, because of its limited abundance and high price, it is a timely and important project to develop low-price materials with a high activity and stability.

Various alternative candidates have shown potential to replace Pt.[4−9] Among them, heteroatom-doped carbon materials are highlighted in terms of their high activity, durability, and low cost.[10−13] Even though the exact reaction mechanisms and the active sites are under debate, these electrocatalysts show possibilities to replace Pt. Especially, N-doped carbons with high surface area, including graphene[14,15] and carbon nanotube,[16,17] show an outstanding activity; considering that electrocatalytic reaction occurs on catalyst surface, exposing more active sites is an unequivocally important issue. In particular, the importance of the microporous area was accentuated because of the rational trend between the microporous area and activity.[18,19] Many advances

in generating micropore structure have been achieved by carbonization of metal-organic framework[20,21] or activation of carbon using NH_3 or KOH.[22,23] However, effective utilization of micropore is another important issue. Because micropores are generally limited in mass transport due to narrow pore, many attempts to enhance the mass transport issues were made by introduction of mesopore structure.[10,24,25] In this sense, hierarchical structures are a promising candidate to achieve both formation and utilization of micropores simultaneously. Due to their unique structural advantages, hierarchical structures have been reported to lead to high activity in various electrochemical reactions.[22,26] Nevertheless, complex synthesis protocols and the limitations in mass production are still large hurdles for effective utilization of carbon-based materials, which are important criteria for practical applications.

In this regard, natural sources are potentially very attractive for carbon materials because of their abundance and facile accessibility. Some organic materials have demonstrated their potential as carbon sources for heteroatom-doped carbon materials for electrochemical applications.[27,28] For example, Wang group suggested successful synthesis and application of active carbon materials using biomass.[29,30] In particular,

Figure 1. Scheme of coffee waste-derived hierarchical nitrogen-doped porous carbon synthesis.

regeneration of byproducts or waste from natural sources is invaluable from both environmental and industrial viewpoints because it converts waste into valuable products. Among various natural sources, coffee beans are one of the largest natural products in the world (almost 7 million tons of coffee beans are produced each year).[31] With the large consumption rate of coffee worldwide, a huge amount of coffee waste (CW) has been generated. However, CW can emit greenhouse gasses, such as methane, during its decomposition in a landfill;[32] therefore, effective utilization of CW is not only an economic issue but also an environmental one. Many efforts have been suggested, including extraction of biodiesel from CW[33] or application of CW to CO_2 capture[34] and supercapacitor electrode materials.[35,36] Nonetheless, considering its large amounts of generation, CW still needs to be recycled and utilized more in a wide variety of fields. In particular, with its abundant sources of nitrogen in caffeine and proteins, we expect that CW can be a promising source for nitrogen-doped carbon as an electrocatalyst for various energy conversion systems.

Here, we suggest a very useful and easy approach for nitrogen-doped porous carbon derived from CW and verify its feasibility as an active and promising material for electrochemical energy devices. Hierarchical porous carbon with a high surface area ($\sim$1200 m^2 g^{-1}) was obtained by one-step heat treatment of a mixture of CW and $ZnCl_2$ in an inert atmosphere. These hierarchical porous carbons, which have both micro- and mesoporous structures, are applied as electrocatalysts for both ORR and IRR. The ORR performance of the carbon material shows activities as high as the state-of-the-art Pt electrocatalyst; its photovoltaic efficiency as a counter electrode (CE) in DSSCs is up to 8.32%, which is even higher than that for Pt (8.07%).

2. RESULTS AND DISCUSSION

2.1. Synthesis of Hierarchical Porous Carbon from Coffee Waste.
The synthesis of nitrogen-doped porous carbon materials from CW was conducted by a single-step carbonization method (Figure 1); CW obtained after coffee brewing was heat-treated under an Ar atmosphere in a tube furnace (see details in the Experimental Section). To modify the physicochemical properties of the carbon materials, the carbonization temperature was controlled from 600 to 900 °C. The product samples are denoted as CCW_T; CCW refers to carbon derived from coffee waste and T indicates the carbonization temperature. In addition, $ZnCl_2$ activation was adopted to create the hierarchical porous structure. $ZnCl_2$ activation is a well-known procedure to generate nanoscale pores in a carbon structure.[37,38] The exact mechanism is unclear, but $ZnCl_2$ has been suggested to degrade the cellulosic structure and induce dehydration, leading to charring and aromatization of carbon, and eventually the creation of pores.[39] Furthermore, the pore size can be controlled from microscale to mesoscale by controlling the $ZnCl_2$ concentration.[40,41] We conducted $ZnCl_2$ activation using $ZnCl_2$ and CW in a mass ratio of 3:1 to form micro−meso hierarchical porous structure for electrochemical applications. For $ZnCl_2$ activation, CW was soaked in a $ZnCl_2$ aqueous solution and dried overnight. The $ZnCl_2$-treated CWs were then carbonized in the tube furnace under an Ar atmosphere; the products are denoted as CCW_AT (where A indicates the $ZnCl_2$ activation). After carbonization, both the CCW_T and CCW_AT samples were thoroughly washed with 6 M HCl to remove any residuals and filtered several times with deionized (DI) water. To confirm the possibility of impurities in samples, which could affect electrochemical performance, X-ray photoelectron spectroscopy (XPS) was measured as shown in Figure S1 and Table S1. There was no metallic features, such as Fe, Co, and Ni, which are considered as active sites for ORR. There are only N-doped carbon features with carbon, nitrogen, oxygen, and very little amount of sulfur. Furthermore, a small amount of Cl was detected. Considering that Cl was also observed in CCW_T without $ZnCl_2$ treatment, we conjectured that Cl was incorporated during HCl washing step (Table S1). After the whole process, we obtained CCW_AT and CCW_T around 30 and 23 wt % yield compared to initial CW, respectively (Table
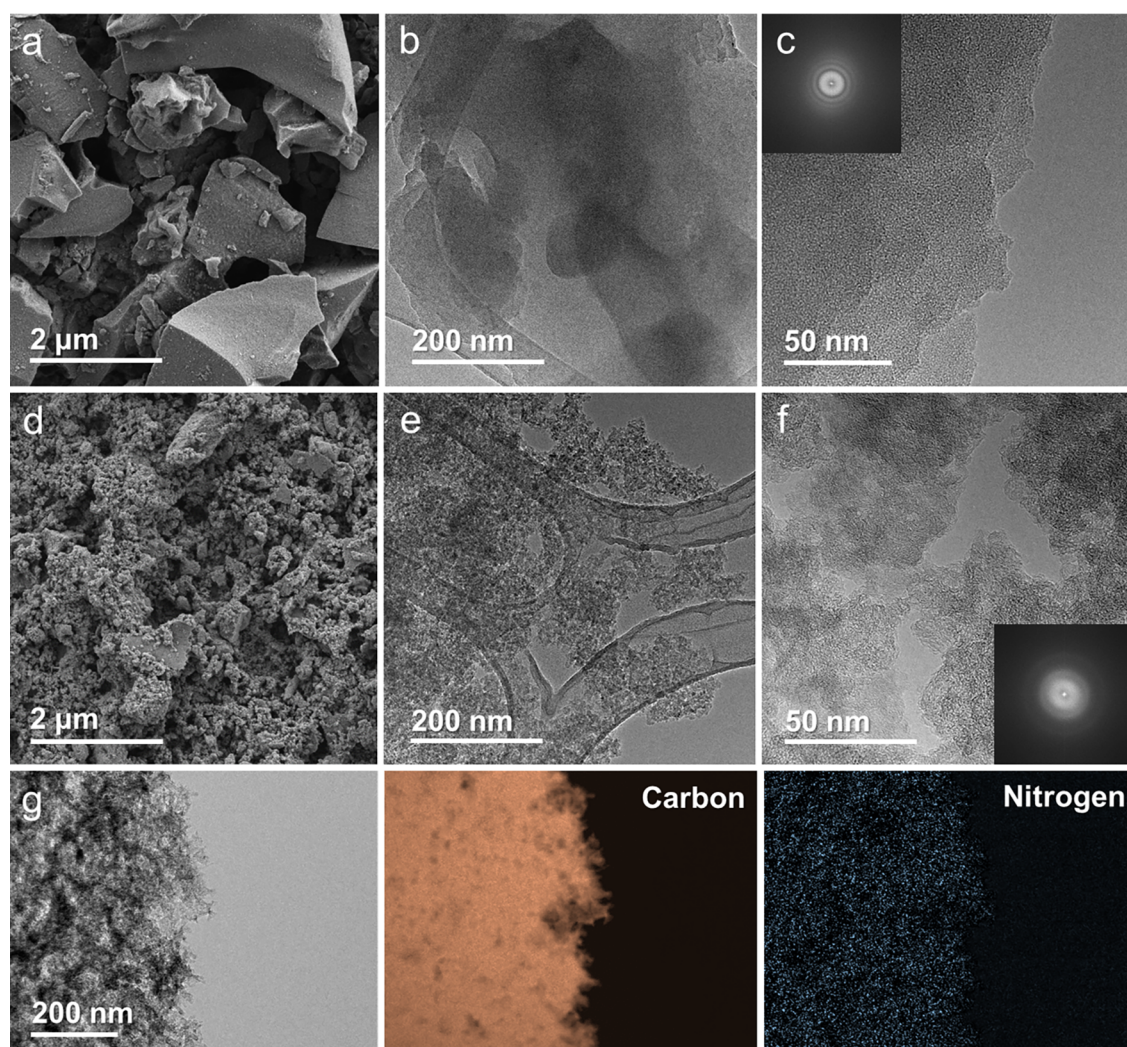
Figure 2. (a) SEM image of CCW_800; (b, c) TEM images of CCW_800; (d) SEM image of CCW_A800; (e, f) TEM images of CCW_A800 (insets of (c) and (f) are FFT images); and (g) EF-TEM images.

S2), which are reasonable values based on thermogravimetric analysis (TGA) result of CCW_T (Figure S2).

Scanning electron microscopy (SEM) and transmission electron microscopy (TEM) images show that the CW is carbonized into chunks of carbon, CCW_T, which are on the order of several micrometers (Figure 2a,b). In contrast, CCW_AT are constructed by small carbon powders of several hundred nanometers (Figure 2d,e). Moreover, while it is hard to discern a porous structure in CCW_T (Figure 2a−c), CCW_AT clearly has a porous structure (Figure 2d−f). The morphological difference by temperature effect cannot be found in both CCW_T and CCW_AT according to TEM analysis (Figure S3). From the fast Fourier transform (FFT) analysis, CCW_T and CCW_AT have an amorphous structure with a low degree of crystallinity (insets of Figure 2c,f), which is further corroborated by X-ray diffraction (XRD) data (Figure S4). Elemental mapping using energy-filtered TEM (EF-TEM) analysis shows that nitrogen is well dispersed in the overall structures, indicating successful nitrogen doping by one-step carbonization (Figure 2g). Nitrogen doping is further confirmed by XPS (Figures 3a and S5). Nitrogen doping was originated from the N content in CW, which is around 2.3 wt % (the N/C ratio is around 4.3 wt %) confirmed by elemental analysis (EA), as shown in Table S3. The exact origin of

nitrogen is unclear, but it is presumed that caffeine and various proteins in coffee beans might be sources for nitrogen doping.

We compare the nitrogen-doping amounts and sites in terms of various carbonization temperatures and the effect of $ZnCl_2$ activation (Figures 3a, S5, and S6). Two significant features are observed. First, the amounts of graphitic nitrogen increase, whereas those of pyridinic and pyrrolic nitrogen decrease as the carbonization temperature increases.[42,43] This trend is supported by previous reports that the thermal stability of nitrogen decreases in the order of graphitic > pyridinic > pyrrolic nitrogen.[44] Second, the nitrogen-doping level decreases for the $ZnCl_2$-activated samples, which is also confirmed by the elemental analysis data (Table S4). The nitrogen content decrease is due to the loss of unstable dopants during the activation process; in effect, the majority of nitrogen loss results from pyridinic and pyrrolic nitrogen, suggesting that relatively unstable nitrogen functional groups are detached from the carbon lattice during the activated carbonization process. The surface area and pore structure of the carbon materials are analyzed by the Brunauer−Emmett−Teller (BET) method using N_2 adsorption−desorption experiments (Figures 3b and S7).

Considering that the largest surface area is 242.3 m^2 g^{-1} (CCW_900), the pore structure cannot be effectively
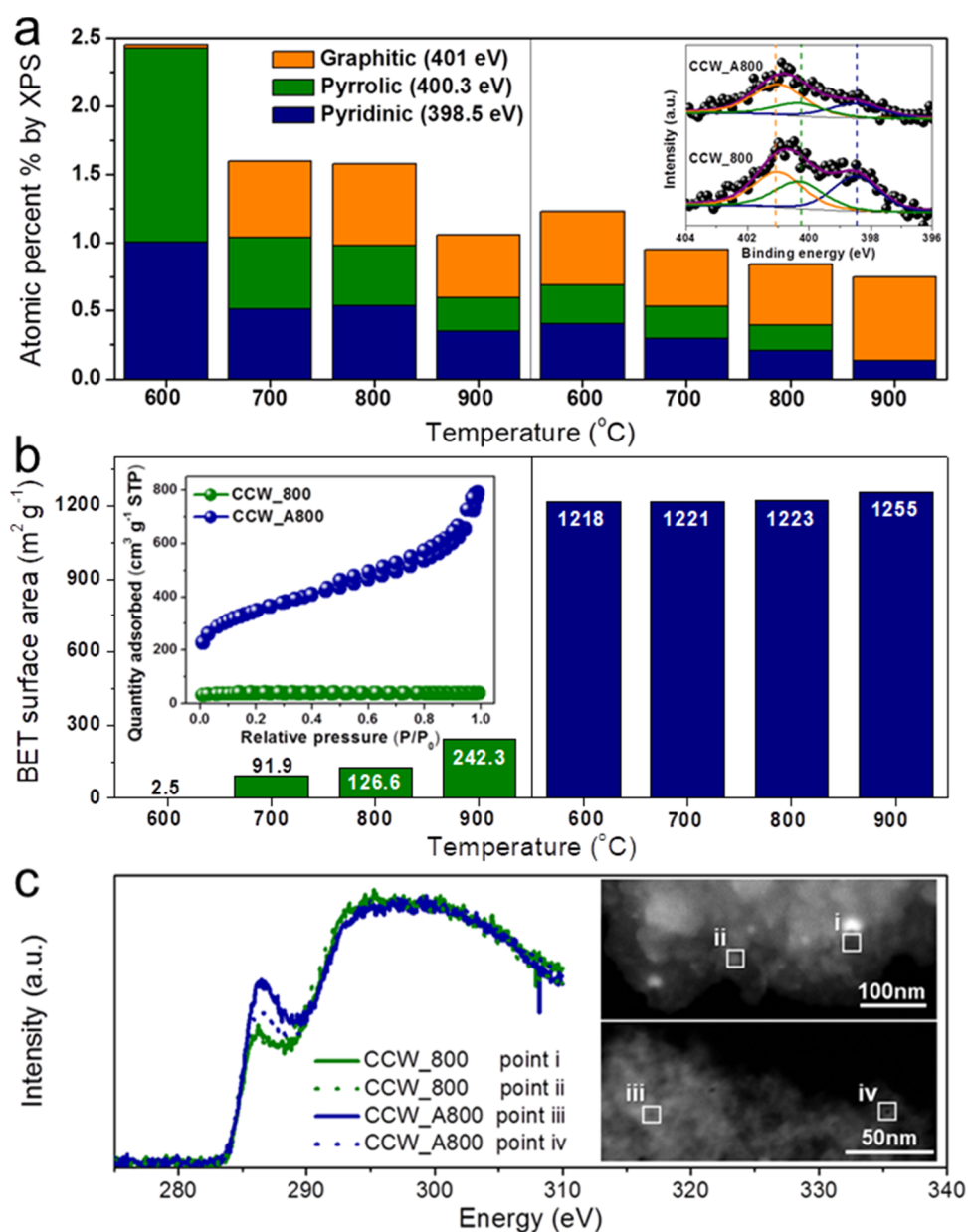
Figure 3. (a) Summary of N 1s XPS fitting results of various CCW_T and CCW_AT samples (inset: N 1s XPS spectra of CCW_800 and CCW_A800). (b) Summary of Brunauer−Emmett−Teller (BET) results of various CCW_T and CCW_AT samples (inset: N_2 adsorption/desorption isotherms of CCW_800 and CCW_A800). (c) Carbon K edge electron energy loss spectroscopy (EELS) spectrum of CCW_800 and CCW_A800 (insets: the EELS measurement points in scanning transmission electron microscopy (STEM) mode).

developed by simple carbonization of CW; on the other hand, the surface areas of all CCW_AT samples are around 1200 m^2 g^{-1}. There is no temperature dependence among the CCW_AT samples, which is reasonable because $ZnCl_2$ activation is known to occur below 600 °C.[45] From the adsorption isotherm (inset of Figure 3b, and Figure S7), CCW_AT shows a 1,4-hybrid-type pore structure, the hierarchical structures of the micropores (d < 2 nm) and mesopores (2 nm < d < 50 nm), which is further supported by the density functional analysis of the BET results (Figure S8), in which micropores (d ≈ 0.8 nm) and mesopores are measured. Formation of the hierarchical structure is attributed to $ZnCl_2$ activation characteristics, where the micro- and mesopores are suggested to be formed simultaneously in case of a mass ratio of $ZnCl_2$ to organic materials > 0.4.[39] We used the Raman spectroscopy to estimate the carbon features of all

samples. As shown in Figure S9, there are no differences between the Raman spectra of CCW_800 and CCW_A800. This is a counterintuitive result because more porous carbon generally shows a higher degree of defective structures (D) than graphitic structures (G).[46,47] To further understand the carbon properties, we measured the carbon K edge electron energy loss spectroscopy (EELS) using scanning transmission electron microscopy (STEM) mode in TEM (Figure 3c). The signals were acquired at two random positions on each sample, as marked in Figure 3c. Interestingly, a higher sp^2 signal was obtained for CCW_A800 than for CCW_800 in spite of the larger surface area of the former. This high sp^2 nature likely originates from the Zn-promoted graphitization of carbon.[48] XRD data also supported that $ZnCl_2$-activated samples have narrower carbon layer distance (positive shift of 002 peak) than nonactivated ones, indicating their higher degree of graphitiza-
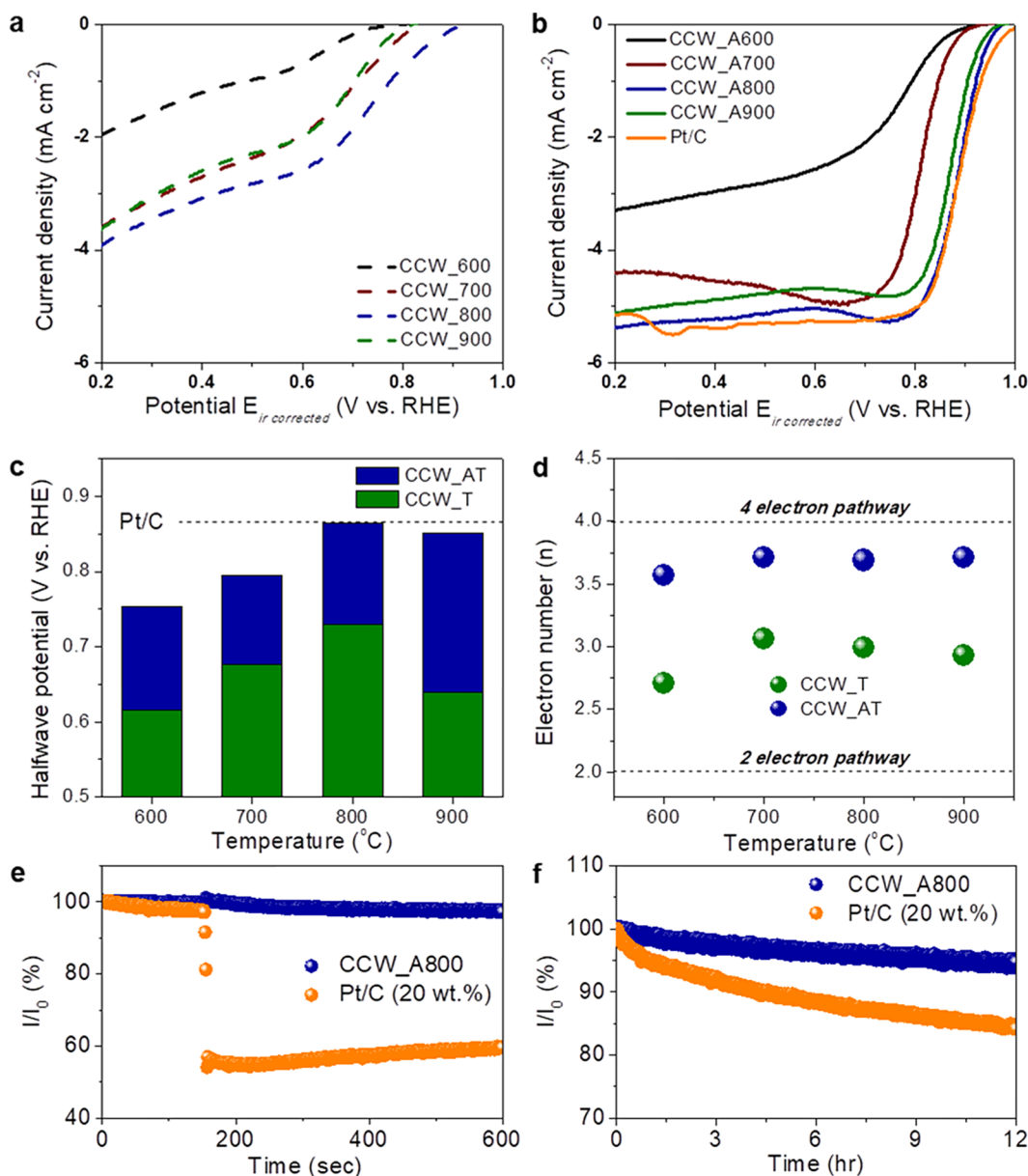
Figure 4. ORR polarization curves of (a) CCW_T and (b) CCW_AT and Pt/C; (c) electron transfer number calculated using the RRDE ring and disk current; (d) summary of the half-wave potential; (e) methanol selectivity test (methanol introduction at 150 s); and (f) and durability test for CCW_A800 and Pt/C.

tion, whereas the grain size of CCW_AT was smaller than that of CCW_T based on their broader peak shape (Figure S10). From both the Raman and EELS analyses, we conclude that the CCW_AT samples have comparable or even higher graphitic carbon textures than CCW_T, even though the CCW_AT samples have much larger surface areas (approximately 8 times larger than that for CCW_T). We expect that this feature is beneficial for electrochemical applications in electrical conductivity.

2.2. Electrochemical Performance of Oxygen Reduction Reaction in Alkaline Media. The electrocatalytic properties were measured using the rotating ring-disk electrode (RRDE) in 0.1 M KOH (Figure 4a,b). The overall ORR activity trends are classified by two features by activity and selectivity. From activity point of view, the activity increases up to 800 °C and slightly decreases in the case of CCW_900 and CCW_A900 (Figure 4c). This trend is understood by the

underlying counterbalance effect between the formation of the effective active site and decrease in absolute amounts of the active site.[49,50] In other words, more active nitrogen sites for ORR are formed with increasing temperature, whereas the absolute nitrogen-doping amounts decrease. To understand which sites are most active for ORR in our samples, we compared the temperature effect and ORR activity of CCW_AT samples, which have similar surface area and pore structure at all temperatures (600−900 °C). With respect to the dopants, the graphitic nitrogen ratio increases as the temperature increases, whereas the amounts of pyridinic and pyrrolic nitrogen groups decrease. From these trends, we expect that graphitic nitrogen has important roles in our samples, whereas the activity loss in the case of CCW_A900 might be due to the low nitrogen-doping level. Compared to previous reports to describe active sites for carbon-based materials, there are still large antithetical results.[51−53] These contradictories are
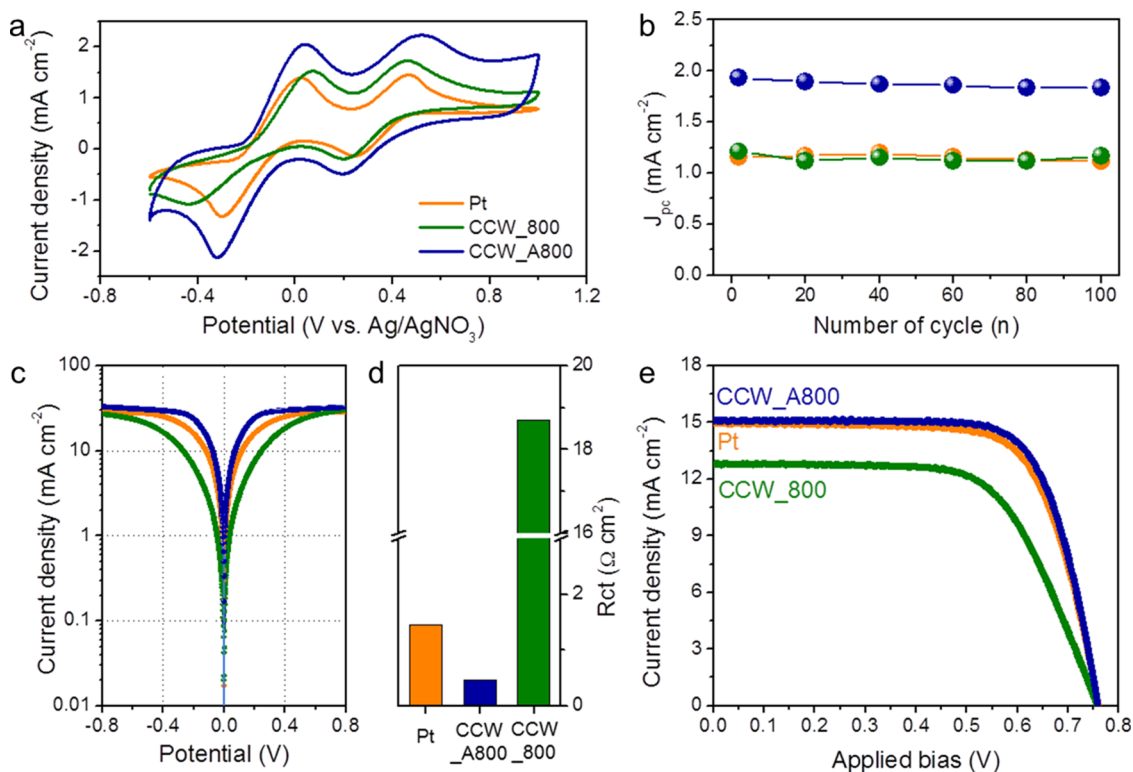
Figure 5. (a) IRR cyclic voltammograms of CCW_800, CCW_A800, and Pt; (b) cathodic peak current density as a function of CV cycle number; (c) Tafel analysis; (d) charge-transfer resistance result based on EIS fitting; and (e) DSSC $J{-}V$ performance curve.

mainly due to difficulties in constructing rational control groups; for model studies, doping sites should be controlled, whereas various factors, including doping level, surface area, pore structure, and conductivity, are identical. As these ambiguities are still big hurdles, we expect that our study based on CCW_AT is a good model to understand the temperature effect because other parameters, such as surface areas and pore structures, are well controlled. However, most significant activity increase was observed depending on not the temperature control but the surface area increase by $ZnCl_2$ activation. The ORR activity of all CCW_AT samples is much higher than that of the CCW_T samples. This significant activity increase of CCW_AT compared to CCW_T can be attributed to the dramatic increase in microporous surface area, which is well supported by previous reports that micropore is highly related to the active sites.[18] Other effects, such as the amounts of nitrogen doping and the ratio between nitrogen-doping sites, cannot sufficiently account for the huge activity increase of CCW_AT. Therefore, we conjecture that surface area engineering is a critical factor for increasing the ORR activity in carbon-based materials, whereas delicate control of active sites by changing dopant concentration in the sites is also a demanding approach.

In terms of reaction selectivity, a dominant four-electron reduction pathway was observed in the case of CCW_AT, whereas CCW_T showed a two-electron dominant pathway (Figures 4d and S11). Considering that selectivity for the four-electron pathway is an important issue for anion exchange membrane fuel cell (AEMFC) because H_2O_2, the product of the two-electron reaction, can attack membrane backbone group and degrade membrane performance,[54] reaction selectivity increase is important as much as activity enhancement. The selectivity enhancement of CCW_AT compared to

CCW_T can be affected by two possibilities. First, the reaction probability enhancement due to the high surface area can result in the four-electron pathway. By increasing the surface area, the probability of reduction of H_2O_2 can be increased, which is a similar effect to catalyst-loading effect for ORR selectivity.[55,56] Changing from a two-electron pathway to a four-electron pathway by increasing the catalyst loading is related to increasing the reactant collision probability by increasing the catalyst layer thickness (not the catalytic site effect). Compared to CCW_AT, CCW_AT has about 8 times higher surface area, which indicates that the probability of reaction collision frequency can be significantly enhanced. Furthermore, micro-porous structure of CCW_AT, which is efficient for confining the reactant in small volumes, may play the key role for enhancing reaction selectivity. Second, active sites for the four-electron pathway can be formed during the activation process. In accordance with the active sites issues, which factors can affect the four-electron pathway is still under debate. Graphitic nitrogen has been suggested by the four-electron pathway active site;[57,58] however, pyridinic nitrogen also has been suggested as an efficient active site.[59,60] In our samples, we cannot find trend to support the selectivity increase of CCW_AT over CCW_T in terms of active-site issues, such as nitrogen-doping level, functionalities, and carbon character among all CCW_T and CCW_AT. For example, if the absolute nitrogen-doping level affects the selectivity, there is no correlation in each CCW_T and CCW_AT samples by temperature change. Moreover, even if significant active sites for the direct four-electron pathway might exist among pyridinic, pyrrolic, or graphitic nitrogen, there is no trend to suggest which sites mainly promote the four-electron pathway. Therefore, we cannot clearly suggest which factors can affect the formation of the four-electron dominant active sites in the

current study. It is unclear which is the main origin for the high selectivity of CCW_AT compared to CCW_T: reaction probability issues or the formation of four-electron active sites. However, on the basis of the fact that drastic selectivity enhancement was observed by the surface area control rather than active-site control issues by temperature effect, we conjecture that high-surface-area engineering is pivotal for enhancing reaction selectivity in carbon-based ORR electrocatalysts.

As a candidate material for renewable fuel cell device, ORR activity of CCW_A800 is comparable to that of the state-of-the-art Pt/C (Figure 4b). The half-wave potential of 0.87 V (vs reversible hydrogen electrode, or RHE) is also comparable to one of the best results reported for metal-free ORR electrocatalysts (Figure 4c and Table S5). The origin of high ORR activity can be attributed to the microporous large surface area effect, as discussed above, and hierarchical structure with the coexistence of mesopores. Recently, Pampel et al. have suggested that the half-wave potential is highly affected by mesopores, opening the bottleneck pores.[25] Our previous paper also suggested the importance of mass transport by mesopores in microporous carbon for ORR activity.[10] For real application, chemical selectivity and long-term durability as well as high catalytic activity are important criteria. Even a small amount of a poisoning species, such as methanol or CO, can block the active surface of the catalysts and decrease the activity. To examine the chemical selectivity, we conducted a methanol selectivity test by deliberately introducing methanol in the electrolyte while performing chronoamperometry under O_2-saturated ORR conditions (Figure 4e). During introducing methanol, there was an abrupt current change in Pt/C, whereas CCW_A800 shows no response at methanol, indicating its potential as an electrocatalyst for direct methanol fuel cell (DMFC) cathode. An electrochemical durability test was conducted by chronoamperometry at 0.8 V. CCW_A800 shows a high stability and retains its initial activity up to 12 h (activity loss, below 5%), whereas Pt/C is deactivated by 15% of its initial activity, which shows the electrochemical robustness of CCW_A800 (Figure 4f).

2.3. Application to Dye-Sensitized Solar Cell. To verify its feasibility for various electrochemical energy applications, CW-derived carbon materials (CCW_800 and CCW_A800) are applied to DSSCs. We also compared the conventional Pt as a reference for performance comparison. The electrocatalytic reaction of the prepared electrodes for IRR was investigated by cyclic voltammetry (CV). As shown in Figure 5a, two clear pairs of redox peaks are observed for each electrode. The pairs of redox peaks at high and low potentials correspond to the redox reactions of I_3^-/I_2 and I^-/I_3^-, respectively.[61] The analogous shape of the CV curves of CCW and Pt indicates their similar electrochemical behaviors. Each CV curve maintained its initial shape and cathodic peak current density without an appreciable loss during 100 consecutive cycles (Figures 5b and S12), validating their stability in IRR. To compare the electrocatalytic activities, Tafel polarization analyses were conducted using symmetrical dummy cells. CCW_A800 shows an obviously larger slope than CCW_800 and even Pt (Figure 5c), indicating higher exchange current density (J_0) and superior electrocatalytic activity.[62] To further reveal the activity trend in a quantitative manner, we conducted electrochemical impedance spectroscopy (EIS) analyses. The EIS results were investigated by the equivalent circuit curve fitting (Figure S13 and Table S6, see Supporting Information

for details related to EIS analysis). As shown in Figure 5d, CCW_A800 exhibited a significantly smaller charge-transfer resistance (R_{ct}) value (0.46 Ω cm^2) compared to CCW_800 (18.69 Ω cm^2) and even Pt (1.46 Ω cm^2). In contrast, series resistance (R_s) and Warburg impedance (W_s) showed no significant differences (Table S6). The J_0 can be estimated from the obtained R_{ct} values using the following equation[63]

$$J_0 = RT/nFR_{ct}$$

The J_0 values increase in the order of CCW_800 < Pt < CCW_A800 and correspond to the activity trend from the Tafel polarization curve. On the basis of the Tafel and EIS analyses, the electrocatalytic activity of CCW_A800 is superior to that of CCW_800 and Pt. The photocurrent density–voltage (J–V) results of DSSC application are shown in Figure 5e, and the photovoltaic parameters are summarized in Table S7. CCW_A800 exhibited a superior photovoltaic efficiency (η = 8.32 ± 0.04%) to CCW_800 (η = 6.25 ± 0.04%) and even to conventional Pt (η = 8.07 ± 0.05%). Given that the open-circuit voltages (V_{oc}) of each electrode were comparable, this superior photovoltaic efficiency for the DSSC with CCW_A800 was owing to the enhanced short-circuit current density (J_{sc} = 15.09 ± 0.04 mA cm^{-2}) and fill factor (FF = 72.6 ± 0.7%). When the CE is the only variable factor in the DSSCs, any FF and J_{sc} improvements arise from the enhanced electrocatalytic activity for IRR.[64,65] The origin of enhanced electrocatalytic activity can be classified by either a superior intrinsic catalytic activity or increased effective active site (or both).[66,67] According to previous reports, there are still controversies on active sites for carbon-based materials; for example, carbon defect sites[68] or nitrogen functional groups,[66,69] such as pyridinic and graphitic nitrogen, are suggested as the main active site. To reveal the activity origin in our samples, we conducted temperature-dependent charge-transfer analysis using EIS to get the information of activation energy for IRR, which is intrinsic parameter apart from the surface area (Figure S14). The R_{ct} and J_0 values from EIS measurements follow the Arrhenius equation

$$J_0 = J_{inf} \exp\left(-\frac{E_a}{RT}\right)$$

where J_{inf} is the exchange current density at infinite temperature and E_a is the activation energy. E_a was calculated from Arrhenius plots (Figure S15 and Table S8). The E_a values of CCW_800 and CCW_A800 are similar but higher compared to that of Pt, indicating that enhanced catalytic activity of CCW_A800 is attributed to not the intrinsic active site but the increase of electrocatalytic active surface area. From the DSSC application, we corroborated the importance of high-surface-area engineering with porous structure of carbon-based materials for electrocatalytic application, and our facile and environment-friendly process can be successfully applied to various electrochemical devices with high activity and stability.

3. CONCLUSIONS

In this study, we demonstrated a very easy and effective design for nitrogen-doped carbon materials using CW. The hierarchical porous structure with mesopores and micropores was constructed by a single-step heat treatment using $ZnCl_2$ without any further activation step or template. These hierarchical porous carbons were applied as the electrocatalysts for both ORR and IRR to validate its feasibility for various

electrochemical energy applications. The obtained ORR performance of the hierarchical porous carbon showed a high activity and stability, which is similar to or even better than state-of-the-art Pt. Also, the half-wave potential was around 870 mV versus RHE, which is comparable to one of the best results reported by metal-free carbon-based materials in alkaline media. Furthermore, high reaction selectivity to four-electron pathway indicates that our porous carbon materials have potential for real application to AEMFC. Finally, our materials also showed potential as a CE electrocatalyst in DSSCs. The photovoltaic efficiency of hierarchical carbon was 8.32%, which is an outstanding value compared to the conventional Pt result (8.07%). We believe that our facile synthetic protocol for obtaining hierarchical porous and nitrogen-doped carbon materials by a single-step heat treatment using natural sources can be further extended to design effective carbon-based electrochemical active materials, such as supercapacitors or rechargeable batteries.

4. EXPERIMENTAL SECTION

4.1. Materials Synthesis and Characterizations. CW (CW is coffee ground waste after brewing coffee) was obtained from commercially available coffee beans. CW-derived carbons were synthesized by a single-step heat treatment carbonization process. Heat treatment was conducted in an Ar flow tube furnace at four different carbonization temperatures (600, 700, 800, and 900 °C). The heating rate was controlled at 5 °C min^{-1}, and each target temperature was maintained for 2 h. CCW_AT was synthesized by carbonization of a CW and ZnCl$_2$ mixture. The mixture was made by soaking the CW into an aqueous ZnCl$_2$ solution (the mass ratio of CW to ZnCl$_2$ is 1:3). After fully evaporating the water, the mixture was placed in an alumina crucible in a tube furnace and the heat treatment was conducted according to the same procedure for CCW_T formation. After carbonization, both the CCW_T and CCW_AT samples were immersed in 6 M HCl overnight to remove the residuals and filtered several times with DI water. After filtration, CCW_T and CCW_AT were fully dried in a 60 °C oven overnight and ground in a mortar. The compositions of CW, CCW_T, and CCW_AT were identified using an elemental analyzer (Flash 1112, Thermo Fisher Scientific). The yield of CCW_T was measured by TGA (SDT Q600, TA instruments), where the temperature was increased to 800 °C at a heating rate of 5 °C min^{-1} under N$_2$ gas flow of 100 mL min^{-1}. Field emission SEM (MERLIN Compact, ZEISS) was used to characterize the morphology of the samples. The TEM images were obtained using a Tecnai F20 instrument at an operation voltage of 200 kV. EELS and energy-filtered TEM images were acquired using a JEOL 2100F instrument at an operation voltage of 200 kV. Powder XRD was performed using a Rigaku D/MAX 2500 spectrometer with a Cu Kα (λ = 0.15418 nm) source. XPS (K-Alpha, Thermo Fisher Scientific) was carried out using Al Kα (1486.6 eV). Raman spectroscopy was performed using a Horiba LabRAM HV Evolution spectrometer with a 532 nm laser. The nitrogen sorption experiment was performed using a Micromeritics TriStar II 3020 surface area and porosity instrument. The pore size distributions of CCW_800 and CCW_A800 were obtained using a BELSORP-max instrument (MicrotracBEL Corp.), and pore size analysis was conducted by nonlocal density functional theory.

4.2. Electrochemical ORR analysis. Electrochemical analysis was performed using an Autolab potentiostat (PGSTAT302N). A carbon rod and Ag/AgCl reference electrode were used as the CE and reference electrode, respectively. All potentials are denoted as RHE scale. An IR-drop correction was conducted. The electrocatalysts, including a commercial Pt/C catalyst (20 wt %, Johnson Matthey Co.), were dispersed with Nafion (15 wt %, Sigma-Aldrich) and 2-propanol. The ink was deposited onto the RRDE (Pine Research, disk area = 0.2475 cm^2). The total catalyst loading of CW-derived carbon and Pt/C was 0.274 mg cm^{-2}. The ORR measurement was conducted

under an O$_2$-saturated 0.1 M KOH electrolyte at 25 °C. To calculate the electron number using RRDE, we used a collection efficiency of 0.37, and the ring voltage was fixed at 1.4 V versus RHE. A long-term durability test was conducted by chronoamperometry at 0.8 V versus RHE under O$_2$-saturated conditions with a rotating speed of 1600 rpm. We conducted a methanol selectivity test by chronoamperometry at 0.7 V versus RHE. During chronoamperometry, 3 mL of pure methanol was introduced in the electrolyte.

4.3. Fabrication of DSSCs. For the preparation of the TiO$_2$ working electrodes (WEs), a TiO$_2$ blocking layer was coated onto the FTO glasses by immersing them in a 40 mM TiCl$_4$ aqueous solution at 70 °C for 30 min. After washing and drying, a colloidal TiO$_2$ paste (DSL 18NR-T, Dyesol Ltd.) was doctor-bladed onto the pretreated FTO glass and annealed at 500 °C for 30 min. After the annealing process, the electrodes were dipped into a 16 mM TiCl$_4$ aqueous solution at 70 °C for 30 min and annealed at 450 °C for 30 min. The resulting TiO$_2$ electrodes were sensitized with cis-bis(isothiocyanato)-bis(2,2'-bipyridyl-4,4-dicarboxylic acid)ruthenium(II) (N719 dye, Ohyoung Industrial Co.) by immersing them in an ethanol solution of 0.5 mM N719 dye at 30 °C for 24 h. The platinum CEs were prepared by spin-coating 300 μL of the Pt precursor solution (50 mM H$_2$PtCl$_6$ in 2-propanol) onto FTO glasses (TEC-8, Pilkington) at 900 rpm. Then, the Pt-coated CEs were heated at 400 °C for 30 min in air to remove the solvents and other impurities. The CW-derived carbon CEs were prepared by the spray method. For the preparation of catalyst ink for spray, carbon catalysts were ground using a mortar and pestle and dispersed in ethanol. Then, the Nafion ionomer (5 wt %, Aldrich) with a 5 wt % ratio was added to the solution, and the solution was ultrasonicated for 30 min. The obtained catalyst ink was sprayed onto the FTO glass and heat-treated at 400 °C for 3 h under an Ar flow. The prepared WEs and CEs were assembled using a 50 μm thick thermoplastic sealant (Surlyn, Dupont). The iodide electrolyte was injected into the assembled cell through a predrilled hole. The iodide and triiodide (I$^-$/I$_3^-$) redox electrolyte for DSSC was composed of 0.6 M 1-butyl-3-methylimidazolium iodide, 30 mM I$_2$, 0.1 M guanidinium thiocyanate, and 0.5 M 4-*tert*-butylpyridine in a mixture of acetonitrile and valeronitrile (volumetric ratio = 85:15). All chemicals mentioned above were purchased from Sigma-Aldrich and used without further purification.

4.4. Electrochemical IRR Analysis and DSSC Performance Evaluation. CV analysis and Tafel polarization plots were measured using a potentiostat (PGSTAT128N, Metrohm Autolab). CV analysis was measured with a three-electrode system using a Pt mesh CE and Ag/AgNO$_3$ reference electrode. For the CV measurements, iodide and triiodide (I$^-$/I$_3^-$) redox electrolytes were prepared by mixing 10 mM LiI, 1 mM I$_2$, and 0.1 M LiClO$_4$ in acetonitrile. CV curves were recorded in the potential range of −0.6 to 1.0 V at scan rates of 50 mV s^{-1}. Symmetric dummy cells for the evaluation of the electrocatalytic activity of the catalysts were fabricated in the same method as DSSC, except that two identical Pt, CCW_800, or CCW_A800 electrodes were assembled. Tafel polarization plots were measured in a symmetric dummy cell using the same electrolyte as that for DSSC and were recorded from −0.8 to 0.8 V at a scan rate of 50 mV s^{-1}. EIS was measured with symmetric dummy cells at temperatures of 283, 293, 303, 313, and 323 K using a multichannel electrochemical workstation (ZIVE MP1). The EIS experiment was performed from 50 mHz to 100 kHz with an AC amplitude of 10 mV and an applied bias voltage of 0 V. The spectral results were fitted with Z-view software. Photovoltaic properties were characterized by solar simulators (XIL model 05A50KS source measure units, SERIC Ltd.) for DSSCs under 1 sun (AM 1.5 G with an incident light intensity of 100 mW cm^{-2}), which was verified by a calibrated Si reference solar cell (National Institute of Advanced Industrial Science and Technology, AIST, Japan). The active area of the dye-sensitized TiO$_2$ film was 0.2025 cm^2. Prior to the photovoltaic measurement, a black aperture mask covered the devices to avoid overestimation of the photovoltaic efficiency.

■ ASSOCIATED CONTENT

Ⓢ Supporting Information

The Supporting Information is available free of charge on the ACS Publications website at DOI: 10.1021/acsami.7b13799.

Additional experimental results of XPS spectra, TGA curve, XRD, BET analysis, Raman spectra, elemental analysis, and EIS analysis available (PDF)

■ AUTHOR INFORMATION

Corresponding Author

*E-mail: ysung@snu.ac.kr.

ORCID Ⓞ

Dong Young Chung: 0000-0001-5453-8314

Yung-Eun Sung: 0000-0002-1563-8328

Author Contributions

§D.Y.C., Y.J.S., J.M.Y. contributed equally to this work.

Notes

The authors declare no competing financial interest.

■ ACKNOWLEDGMENTS

■ REFERENCES

(1) Chen, C.; Kang, Y.; Hou, Z.; Zhu, Z.; Huang, W.; Xin, H. L.; Snyder, J. D.; Li, D.; Herron, J. A.; Mavrikakis, M.; Chi, M.; More, K. L.; Li, Y.; Markovic, N. M.; Somorjai, G. A.; Yang, P.; Stamenkovic, V. R. Highly Crystalline Multimetallic Nanoframes with Three-Dimensional Electrocatalytic Surfaces. *Science* **2014**, *343*, 1339−1343.

(2) Chung, D. Y.; Jun, S. W.; Yoon, G.; Kwon, S. G.; Shin, D. Y.; Seo, P.; Yoo, J. M.; Shin, H.; Chung, Y. H.; Kim, H.; Mun, B. S.; Lee, K.-S.; Lee, N.-S.; Yoo, S. J.; Lim, D.-H.; Kang, K.; Sung, Y.-E.; Hyeon, T. Highly Durable and Active PtFe Nanocatalyst for Electrochemical Oxygen Reduction Reaction. *J. Am. Chem. Soc.* **2015**, *137*, 15478−15485.

(3) Yun, S.; Hagfeldt, A.; Ma, T. Pt-Free Counter Electrode for Dye-Sensitized Solar Cells with High Efficiency. *Adv. Mater.* **2014**, *26*, 6210−6237.

(4) Wu, G.; More, K. L.; Johnston, C. M.; Zelenay, P. High-performance Electrocatalysts for Oxygen Reduction Derived from Polyaniline, Iron, and Cobalt. *Science* **2011**, *332*, 443−337.

(5) Lefèvre, M.; Proietti, E.; Jaouen, F.; Dodelet, J.-P. Iron-based Catalysts with Improved Oxygen Reduction Activity in Polymer Electrolyte Fuel Cells. *Science* **2009**, *324*, 71−74.

(6) Shui, J.; Chen, C.; Grabstanowicz, L.; Zhao, D.; Liu, D. J. Highly Efficient Nonprecious Metal Catalyst Prepared with Metal-Organic Framework in a Continuous Carbon Nanofibrous Network. *Proc. Natl. Acad. Sci. U.S.A.* **2015**, *112*, 10629−10634.

(7) Zitolo, A.; Goellner, V.; Armel, V.; Sougrati, M.-T.; Mineva, T.; Stievano, L.; Fonda, E.; Jaouen, F. Identification of Catalytic Sites for Oxygen Reduction in Iron- and Nitrogen-Doped Graphene Materials. *Nat. Mater.* **2015**, *14*, 937−942.

(8) Hou, Y.; Wang, D.; Yang, X. H.; Fang, W. Q.; Zhang, B.; Wang, H. F.; Lu, G. Z.; Hu, P.; Zhao, H. J.; Yang, H. G. Rational Screening Low-Cost Counter Electrodes for Dye-Sensitized Solar Cells. *Nat. Commun.* **2013**, *4*, No. 1583.

(9) Zhang, Z.; Qin, Y.; Dou, M.; Ji, J.; Wang, F. One-step Conversion from Ni/Fe Polyphthalocyanine to N-doped Carbon Supported Ni-Fe Nanoparticles for Highly Efficient Water Splitting. *Nano Energy* **2016**, *30*, 426−433.

(10) Chung, D. Y.; Lee, K. J.; Yu, S.-H.; Kim, M.; Lee, S. Y.; Kim, O.-H.; Park, H.-J.; Sung, Y.-E. Alveoli-Inspired Facile Transport Structure of N-Doped Porous Carbon for Electrochemical Energy Applications. *Adv. Energy Mater.* **2014**, *5*, No. 1401309.

(11) Qu, L.; Liu, Y.; Baek, J.-B.; Dai, L. Nitrogen-Doped Graphene as Efficient Metal-Free Electrocatalyst for Oxygen Reduction in Fuel Cells. *ACS Nano* **2010**, *4*, 1321−1326.

(12) Sa, Y. J.; Park, C.; Jeong, H. Y.; Park, S.-H.; Lee, Z.; Kim, K. T.; Park, G.-G.; Joo, S. H. Carbon Nanotubes/Heteroatom-Doped Carbon Core-Sheath Nanostructures as Highly Active, Metal-Free Oxygen Reduction Electrocatalysts for Alkaline Fuel Cells. *Angew. Chem., Int. Ed.* **2014**, *53*, 4102−4106.

(13) Ju, M. J.; Jeon, I.-Y.; Kim, J. C.; Lim, K.; Choi, H.-J.; Jung, S.-M.; Choi, I. T.; Eom, Y. K.; Kwon, Y. J.; Ko, J.; Lee, J.-J.; Kim, H. K.; Baek, J.-B. Graphene Nanoplatelets Doped with N at its Edges as Metal-Free Cathodes for Organic Dye-Sensitized Solar Cells. *Adv. Mater.* **2014**, *26*, 3055−3062.

(14) Li, Y.; Zhou, W.; Wang, H.; Xie, L.; Liang, Y.; Wei, F.; Idrobo, J.; Pennycook, S. J.; Dai, H. An Oxygen Reduction Electrocatalyst Based on Carbon Nanotube-Graphene Complexes. *Nat. Nanotechnol.* **2012**, *7*, 394−400.

(15) Choi, C. H.; Lim, H.-K.; Chung, M. W.; Park, J. C.; Shin, H.; Kim, H.; Woo, S. I. Long-Range Electron Transfer over Graphene-Based Catalyst for High-Performing Oxygen Reduction Reactions: Importance of Size, N-doping, and Metallic Impurities. *J. Am. Chem. Soc.* **2014**, *136*, 9070−9077.

(16) Chung, H. T.; Won, J. H.; Zelenay, P. Active and Stable Carbon Nanotube/Nanoparticle Composite Electrocatalyst for Oxygen Reduction. *Nat. Commun.* **2013**, *4*, No. 1922.

(17) Gong, K.; Du, F.; Xia, Z.; Durstock, M.; Dai, L. Nitrogen-Doped Carbon Nanotube Arrays with High Electrocatalytic Activity for Oxygen Reduction. *Science* **2009**, *323*, 760−764.

(18) Jaouen, F.; Herranz, J.; Lefevre, M.; Dodelet, J.; Kramm, U. I.; Herrmann, I.; Bogdanoff, P.; Maruyama, J.; Nagaoka, T.; Garsuch, A.; Dahn, J. R.; Olson, T.; Pylypenko, S.; Atanassov, P.; Ustinov, E. A. Cross-Laboratory Experimental Study of Non-Noble-Metal Electrocatalysts for the Oxygen Reduction Reaction. *ACS Appl. Mater. Interfaces* **2009**, *1*, 1623−1639.

(19) Jaouen, F.; Lefevre, M.; Dodelet, J.-P.; Cai, M. Heat-Treated Fe/N/C Catalysts for O₂ Electroreduction: Are Active Sites Hosted in Micropores? *J. Phys. Chem. B* **2006**, *110*, 5553−5558.

(20) Zhao, D.; Shui, J.-L.; Grabstanowicz, L. R.; Chen, C.; Commet, S. M.; Xu, T.; Lu, J.; Liu, D.-J. Highly Efficient Non-Precious Metal Electrocatalysts Prepared from One-Pot Synthesized Zeolitic Imidazolate Frameworks. *Adv. Mater.* **2014**, *26*, 1093−1097.

(21) Zhong, H.-x.; Wang, J.; Zhan, Y.; Xu, W.; Xing, W.; Xu, D.; Zhang, Y.; Zhang, X. ZIF-8 Derived Graphene-Based Nitrogen-Doped Porous Carbon Sheets as Highly Efficient and Durable Oxygen Reduction Electrocatalysts. *Angew. Chem., Int. Ed.* **2014**, *53*, 14235−14239.

(22) Liang, H. W.; Zhuang, X.; Bruller, S.; Feng, X.; Mullen, K. Hierarchically Porous Carbons with Optimized Nitrogen Doping as Highly Active Electrocatalysts for Oxygen Reduction. *Nat. Commun.* **2014**, *5*, No. 4973.

(23) Higgins, D.; Chen, Z.; Lee, D. U.; Chen, Z. Activated and Nitrogen-Doped Exfoliated Graphene as Air Electrodes for Metal-Air Battery Applications. *J. Mater. Chem. A* **2013**, *1*, 2639−2645.

(24) Tang, J.; Liu, J.; Li, C.; Li, Y.; Tade, M. O.; Dai, S.; Yamauchi, Y. Synthesis of Nitrogen-Doped Mesoporous Carbon Spheres with Extra-Large Pores Through Assembly of Diblock Copolymer Micelles. *Angew. Chem., Int. Ed.* **2015**, *54*, 588−593.

(25) Pampel, J.; Fellinger, T. Opening of Bottleneck Pores for the Improvement of Nitrogen Doped Carbon Electrocatalysts. *Adv. Energy Mater.* **2016**, *6*, No. 1502389.

(26) Tao, H.; Li, Y.; Jiang, X.; Tang, J.; Wang, Z.; Qian, H.; Mei, P.; Malgras, V.; Bando, Y.; Yamauchi, Y. Perfectly Ordered Mesoporous Iron-Nitrogen Doped Carbon as Highly Efficient Catalyst for Oxygen Reduction Reaction in Both Alkaline and Acidic Electrolytes. *Nano Energy* **2017**, *36*, 286−294.

(27) Li, J.; Zhang, Y.; Zhang, X.; Han, J.; Wang, Y.; Gu, L.; Zhang, Z.; Wang, X.; Jian, J.; Xu, P.; Song, B. Direct Transformation from Graphitic C_3N_4 to Nitrogen-Doped Graphene: An Efficient Metal-Free Electrocatalyst for Oxygen Reduction Reaction. *ACS Appl. Mater. Interfaces* 2015, 7, 19626−19634.

(28) Li, J.; Zhang, Y.; Zhang, X.; Huang, J.; Han, J.; Zhang, Z.; Han, X.; Xu, P.; Song, B. S,N Dual-Doped Graphene-like Carbon Nanosheets as Efficient Oxygen Reduction Reaction Electrocatalysts. *ACS Appl. Mater. Interfaces* 2017, 9, 398−405.

(29) Zhang, Z.; Gao, X.; Dou, M.; Ji, J.; Wang, F. Biomass Derived N-doped Porous Carbon Supported Single Fe Atoms as Superior Electrocatalysts for Oxygen Reduction. *Small* 2017, 13, No. 1604290.

(30) Zhang, Z.; Gao, X.; Dou, M.; Ji, J.; Wang, F. Fe-N_x Moiety-Modified Hierarchically Porous Carbons Derived from Porphyra for Highly Effective Oxygen Reduction Reaction. *J. Mater. Chem. A* 2017, 5, 1526−1532.

(31) Zuorro, A.; Lavecchi, R. Spent Coffee Grounds as a Valuable Source of Phenolic Compounds and Bioenergy. *J. Clean. Prod.* 2012, 34, 49−56.

(32) Powell, J. T.; Townsend, T. G.; Zimmerman, J. B. Estimates of Solid Waste Disposal Rates and Reduction Targets for Landfill Gas Emissions. *Nat. Clim. Change* 2016, 6, 162−166.

(33) Kondamudi, N.; Mohapatra, S. K.; Misra, M. Spent Coffee Grounds as a Versatile Source of Green Energy. *J. Agric. Food Chem.* 2008, 56, 11757−11760.

(34) Plaza, M. G.; Gonzalez, A. S.; Pevida, C.; Pis, J. J.; Rubiera, F. Valorisation of Spent Coffee Grounds as CO_2 Adsorbents for Postcombustion Capture Applications. *Appl. Energy* 2012, 99, 272−279.

(35) Park, M. H.; Yun, Y. S.; Cho, S. Y.; Kim, N. R.; Jin, H.-J. Waste Coffee Grounds-Derived Nanoporous Carbon Nanosheets for Supercapacitors. *Carbon Lett.* 2016, 19, 66−71.

(36) Ramasahayam, S. K.; Clark, A. L.; Hicks, Z.; Viswanathan, T. Spent Coffee Grounds Derived P, N Co-Doped C as Electrocatalyst for Supercapacitor Applications. *Electrochim. Acta* 2015, 168, 414−422.

(37) Zhang, G.; Luo, H.; Li, H.; Wang, L.; Han, B.; Zhang, H.; Li, Y.; Chang, Z.; Kuang, Y.; Sun, X. ZnO-Promoted Dechlorination for Hierarchically Nanoporous Carbon as Superior Oxygen Reduction Electrocatalyst. *Nano Energy* 2016, 26, 241−247.

(38) Subramanian, V.; Luo, C.; Stephan, A. M.; Nahm, K. S.; Thomas, S.; Wei, B. Supercapacitors from Activated Carbon Derived from Banana Fibers. *J. Phys. Chem. C* 2007, 111, 7527−7531.

(39) Molina-Sabio, M.; Rodriguez-Reionoso, F. Role of Chemical Activation in the Development of Carbon Porosity. *Colloids Surf., A* 2004, 241, 15−25.

(40) Hu, Z.; Srinivasan, M. P.; Ni, Y. Novel Activation Process for Preparing Highly Microporous and Mesoporous Activated Carbons. *Carbon* 2001, 39, 877−886.

(41) Catutrla, F.; Molina-Sabio, M.; Rodriguez-Reionoso, F. Preparation of Activated Carbon by Chemical Activation with $ZnCl_2$. *Carbon* 1991, 29, 999−1007.

(42) Zhang, X.; Xu, H.; Li, X.; Li, Y.; Yang, T.; Liang, Y. Facile Synthesis of Nickel-Iron/Nanocarbon Hybrids as Advanced Electrocatalysts for Efficient Water Splitting. *ACS Catal.* 2016, 6, 580−588.

(43) Wang, J.; Ciucci, F. Boosting Bifunctional Oxygen Electrolysis for N-Doped Carbon via Bimetal Addition. *Small* 2017, 13, No. 1604103.

(44) Chen, S.; Bi, J.; Zhao, Y.; Yang, L.; Zhang, C.; Ma, Y.; Wu, Q.; Wang, X.; Hu, Z. Nitrogen-Doped Carbon Nanocages as Efficient Metal-Free Electrocatalysts for Oxygen Reduction Reaction. *Adv. Mater.* 2012, 24, 5593−5597.

(45) Hayashi, J.; Kazehaya, A.; Muroyama, K.; Watkinson, A. P. Nitrogen-Doped Carbon Nanocages as Efficient Metal-Free Electrocatalysts for Oxygen Reduction Reaction. *Carbon* 2000, 38, 1873−1878.

(46) Bokobza, L.; Bruneel, J.-L.; Couzi, M. Raman Spectra of Carbon-Based Materials (from Graphite to Carbon Black) and of Some Silicone Composites. *C* 2015, 1, 77−94.

(47) Khan, U.; O'Neill, A.; Lotya, M.; De, S.; Coleman, J. N. High-Concentration Solvent Exfoliation of Graphene. *Small* 2010, 6, 864−871.

(48) Armel, V.; Hindocha, S.; Salles, F.; Bennett, S.; Jones, D.; Jaouen, F. Structural Descriptors of Zeolitic-Imidazolate Frameworks are Keys to the Activity of Fe-N-C Catalysts. *J. Am. Chem. Soc.* 2017, 139, 453−464.

(49) Chaudhari, N. K.; Song, M. Y.; Yu, J. S. Heteroatom-Doped Highly Porous Carbon from Human Urine. *Sci. Rep.* 2014, 4, No. 5221.

(50) Li, N.; Hu, C.; Ren, L.; Cao, M. Temperature-Dependent Enhancement of Oxygen Reduction Reaction Activity for Interconnected Nitrogen-Doped Carbon Shell. *CrystEngComm* 2013, 15, 8504−8510.

(51) Guo, D.; Shibuya, R.; Akiba, C.; Saji, S.; Kondo, T.; Nakamura, J. Active Sites of Nitrogen-Doped Carbon Materials for Oxygen Reduction Reaction Clarified Using Model Catalysts. *Science* 2016, 351, 361−365.

(52) Sharifi, T.; Hu, G.; Jia, X.; Wagberg, T. Formation of Active Sites for Oxygen Reduction Reactions by Transformation of Nitrogen Functionalities in Nitrogen-Doped Carbon Nanotubes. *ACS Nano* 2012, 6, 8904−8912.

(53) Xing, T.; Zheng, Y.; Li, L. H.; Cowie, B. C. C.; Gunzelmann, D.; Qiao, S. Z.; Huang, S.; Chen, Y. Observation of Active Sites for Oxygen Reduction Reaction on Nitrogen-Doped Multilayer Graphene. *ACS Nano* 2014, 8, 6856−6862.

(54) Varcoe, J. R.; Atanassov, P.; Dekel, D. R.; Herring, A. M.; Hickner, M. A.; Kohl, P. A.; Kucernak, A. R.; Mustain, W. E.; Nijmeijer, K.; Scott, K.; Xu, T.; Zhuang, L. Anion-Exchange Membranes in Electrochemical Energy Systems. *Energy Environ. Sci.* 2014, 7, 3135−3191.

(55) Bonakdarpour, A.; Lefevre, M.; Yang, R.; Jaouen, F.; Dahn, T.; Dodelet, J.-P.; Dahn, J. R. Impact of Loading in RRDE Experiments on Fe-N-C Catalysts: Two- or Four-Electron Oxygen Reduction? *Electrochem. Solid-State Lett.* 2008, 11, B105−B108.

(56) Biddinger, E. J.; Deak, D. V.; Singh, D.; Marsh, H.; Tan, B.; Knapke, D. S.; Ozkan, U. S. Examination of Catalyst Loading Effects on the Selectivity of CN_x and Pt/VC ORR Catalysts Using RRDE. *J. Electrochem. Soc.* 2011, 158, B402−B409.

(57) Silva, R.; Voiry, D.; Chhowalla, M.; Asefa, T. Efficient Metal-Free Electrocatalysts for Oxygen Reduction: Polyaniline-Derived N- and O-Doped Mesoporous Carbons. *J. Am. Chem. Soc.* 2013, 135, 7823−7826.

(58) Kim, O.-H.; Cho, Y.-H.; Chung, D. Y.; Kim, M. J.; Yoo, J. M.; Park, J. E.; Choe, H.; Sung, Y.-E. Facile and Gram-Scale Synthesis of Metal-Free Catalysts: Toward Realistic Applications for Fuel Cells. *Sci. Rep.* 2015, 5, No. 8376.

(59) Wu, J.; Ma, L.; Yadav, R. M.; Yang, Y.; Zhang, X.; Vajtai, R.; Lou, J.; Ajayan, P. M. Nitrogen-Doped Graphene with Pyridinic Dominance as a Highly Active and Stable Electrocatalyst for Oxygen Reduction. *ACS Appl. Mater. Interfaces* 2015, 7, 14763−14769.

(60) Yasuda, S.; Yu, L.; Kim, J.; Murakoshi, K. Selective Nitrogen Doping in Graphene for Oxygen Reduction Reactions. *Chem. Commun.* 2013, 49, 9627−9629.

(61) Wang, Y.; Wu, M.; Lin, X.; Shi, Z.; Hagfeldt, A.; Ma, T. Several Highly Efficient Catalysts for Pt-Free and FTO-Free Counter Electrodes of Dye-Sensitized Solar Cells. *J. Mater. Chem.* 2012, 22, 4009−4014.

(62) Kang, J. S.; Park, M.-A.; Kim, J.-Y.; Park, S. H.; Chung, D. Y.; Yu, S.-H.; Kim, J.; Park, J.; Choi, J.-W.; Lee, K. Y.; Jeong, J.; Ko, M. J.; Ahn, K.-S.; Sung, Y.-E. Reactively Sputtered Nickel Nitride as Electrocatalytic Counter Electrode for Dye- And Quantum Dot-Sensitized Solar Cells. *Sci. Rep.* 2015, 5, No. 10450.

(63) Kavan, L.; Yum, J. H.; Grätzel, M. Graphene Nanoplatelets Outperforming Platinum as the Electrocatalyst in Co-Bipyridine-Mediated Dye-Sensitized Solar Cells. *Nano Lett.* 2011, 11, 5501−5506.

(64) Das, S.; Sudhagar, P.; Verma, V.; Song, D.; Ito, E.; Lee, S. Y.; Kang, Y. S.; Choi, W. Amplifying Charge-Transfer Characteristics of

Graphene for Triiodide Reduction in Dye-Sensitized Solar Cells. *Adv. Funct. Mater.* **2011**, *21*, 3729−3736.

(65) Hou, S.; Cai, X.; Wu, H.; Yu, X.; Peng, M.; Yan, K.; Zou, D. Nitrogen-Doped Graphene for Dye-Sensitized Solar Cells and the Role of Nitrogen States in Triiodide Reduction. *Energy Environ. Sci.* **2013**, *6*, 3356−3362.

(66) Burschka, J.; Brault, V.; Ahmad, S.; Breau, L.; Nazeeruddin, M. K.; Marsan, B.; Zakeeruddin, S. M.; Grätzel, M. Influence of the Counter Electrode on the Photovoltaic Performance of Dye-Sensitized Solar Cells Using a Disulfide/Thiolate Redox Electrolyte. *Energy Environ. Sci.* **2012**, *5*, 6089−6097.

(67) Hoffeditz, W. L.; Katz, M. J.; Deria, P.; Martinson, A. B. F.; Pellin, M. J.; Farha, O. K.; Hupp, J. T. High-Surface-Area Architectures for Improved Charge Transfer Kinetics at the Dark Electrode in Dye-Sensitized Solar Cells. *ACS Appl. Mater. Interfaces* **2014**, *6*, 8646−8650.

(68) Kavan, L.; Yum, J. H.; Grätzel, M. Optically Transparent Cathode for Dye-Sensitized Solar Cells Based on Graphene Nano-platelets. *ACS Nano* **2011**, *5*, 165−172.

(69) Shrestha, A.; Batmunkh, M.; Shearer, C. J.; Yin, Y.; Andersson, G. G.; Shapter, J. G.; Qiao, S.; Dai, S. Nitrogen-Doped CN_x/CNTs Heteroelectrocatalysts for Highly Efficient Dye-Sensitized Solar Cells. *Adv. Energy Mater.* **2017**, *7*, No. 1602276.